JOURNAL OF VIROLOGY, Sept. 1990, p. 4313–4320
0022-538X/90/094313-08$02.00/0

Vol. 64, No. 9

Comparison of Rous Sarcoma Virus RNA Processing in Chicken and Mouse Fibroblasts: Evidence for Double-Spliced RNA in Nonpermissive Mouse Cells

STANTON L. BERBERICH,[1] MIMI MACIAS,[2] LEI ZHANG,[2] LUBOMIR P. TUREK,[3,4] AND C. MARTIN STOLTZFUS[2]*

Program in Genetics[1] and Departments of Microbiology[2] and Pathology,[3] University of Iowa, and Veterans Administration Medical Center,[4] Iowa City, Iowa 52242

Received 30 January 1990/Accepted 5 June 1990

Rous sarcoma virus, an avian retrovirus, transforms but does not replicate in mammalian cells. To determine to what extent differences in RNA splicing might contribute to this lack of productive infection, cloned proviral DNA derived from the Prague A strain of Rous sarcoma virus was transfected into mouse NIH 3T3 cells, and the viral RNA was compared by RNase protection with viral RNA from transfected chicken embryo fibroblasts by using a tandem antisense riboprobe spanning the three major splice sites. The levels of viral RNA in NIH 3T3 cells compared with those in chicken embryo fibroblasts were lower, but the RNA was spliced at increased efficiency. The difference in the ratio of unspliced to spliced RNA levels was not due to the increased lability of unspliced RNA in NIH 3T3 cells. Although chicken embryo fibroblasts contained equal levels of *src* and *env* mRNAs, spliced viral mRNAs in NIH 3T3 cells were almost exclusively *src*. In NIH 3T3 cells the *env* mRNA was further processed by using a cryptic 5′ splice site located within the *env* coding sequences and the normal *src* 3′ splice site to form a double-spliced mRNA. This mRNA was identical to the *src* mRNA, except that a 159-nucleotide sequence from the 5′ end of the *env* gene was inserted at the *src* splice junction. Smaller amounts of single-spliced RNA were also present in which only the region between the cryptic 5′ and *src* 3′ splice sites was spliced out. The aberrant processing of the viral *env* mRNA in NIH 3T3 cells may in part explain the nonpermissiveness of these cells to productive Rous sarcoma virus infection.

Rous sarcoma virus (RSV) is an oncogenic avian retrovirus that undergoes nonpermissive infections in mammalian cells. When RSV is introduced into mammalian cells, either by infection with certain strains of RSV (1, 10, 33–35) or by transfection of viral DNA (7, 26), occasional clones arise that show a transformed phenotype. In these cell lines, integrated copies of proviral DNA are present in the host chromosomes (34, 35), and a low level of unprocessed *gag* precursor Pr76 is produced (11, 36, 37). However, neither infectious nor noninfectious particles are produced (21, 32). However, infectious virus can be rescued from RSV-transformed mammalian cell lines by fusion with permissive chicken embryo fibroblasts (CEF) (5, 15, 24, 31, 32). The levels of viral RNA in RSV-transformed mammalian cell lines are 1 to 3 orders of magnitude lower than those in infected CEF (3, 6, 19). The predominant viral RNA species in these transformed mammalian cell lines is spliced *src* mRNA; only small amounts of unspliced and *env* mRNA are present as well as minor amounts of several other unidentified RNAs (8, 9, 19).

It is not clear to what extent selection for rare transformants in a population of infected cells might affect the types and quantitative distributions of mRNAs in RSV-transformed cells. To avoid this selective bias, we examined viral RNA from NIH 3T3 cells transfected with proviral DNA clones of the Prague A strain of RSV. Also, a comparison of RNA processing of transcripts from a molecularly cloned RSV genome in cells derived from different species should provide information about the maintenance of balanced splicing in different types of infected cells (for a review, see reference 25).

* Corresponding author.

In this report we show that there is a marked increase in the efficiency of splicing of the viral RNAs in NIH 3T3 cells relative to CEF and that NIH 3T3 cells efficiently use a cryptic 5′ splice site (5′ss) within the *env* coding sequence which is silent in CEF. The activation of the *env* 5′ss in NIH 3T3 cells leads to further processing, resulting in the production of two different forms of the *src* mRNA. This may have implications for the expression of *src* in mammalian cells. It may also account in part for the lack of permissiveness in mouse cells for virus replication.

MATERIALS AND METHODS

Plasmids. pJD100, an infectious nonpermuted proviral clone of a Prague A strain of RSV contained in pBR322, was obtained as a gift from J. Thomas Parsons, Department of Microbiology, University of Virginia, Charlottesville. The RNase mapping templates pMap47 and pMap#10 (Fig. 1) were constructed and characterized (Berberich and Stoltzfus, unpublished data). Plasmid pMPM13, a mutant at the *src* 3′ splice site (3′ss), was constructed in the following manner. A subclone of pJD100 that contained the sequence from the *Sac*I site at nucleotide (nt) 6865 to the *Tth*III-1 site at 7330 was cleaved with *Pst*I (single site at nucleotide 7048), treated with T4 DNA polymerase in the presence of the four deoxyribonucleotides to remove the 3′ extensions, and blunt end ligated. The *Sac*I-*Nae*I fragment (nucleotides 6865 to 7169) was then inserted into pJD100 to create pMPM13. During this cloning step, a small deletion in the *src* exon was also created that altered the protected RNA fragments in the RNase mapping experiments (see Results).

Cell culture and DNA transfections. Secondary CEF isolated from embryonated eggs that were negative for both group-specific antigen and chicken-helper factor (SPAFAS,

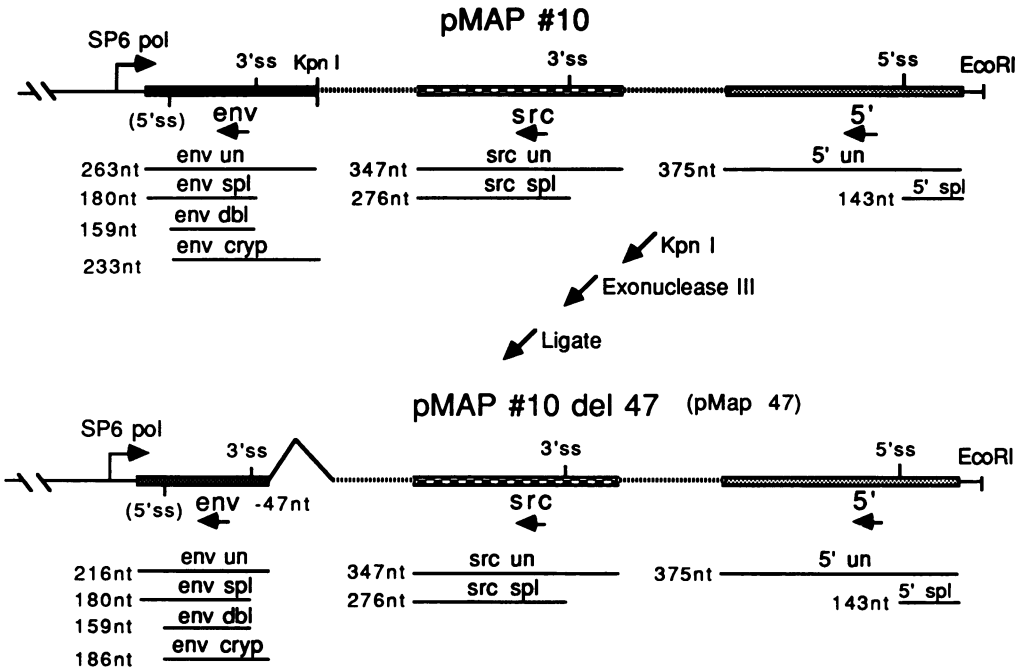

FIG. 1. Maps of riboprobe templates. Plasmid pMap#10 was constructed by ligation of the fragments spanning the *env* 3'ss (nt 4995 to 5258), *src* 3'ss (nt 6983 to 7330), and 5'ss (nt 255 to 630) into plasmid pSP18 containing the SP6 promoter. Plasmid pMap#10 del47 (pMap47) was derived from pMap10 as shown. The plasmids were linearized with *Eco*RI as shown. The sizes of the protected fragments resulting from the two templates are indicated below each plasmid map. Nucleotide numbers are according to the RSV Prague C sequence (20).

Inc., Norwich, Conn.) were cultured in medium 199 (Bethesda Research Laboratories, Inc., Gaithersburg, Md.) supplemented with 10% (vol/vol) tryptose phosphate broth and 5% (vol/vol) calf serum (SGM). Mouse NIH 3T3 cells were cultured in Dulbecco minimum Eagle medium containing 10% (vol/vol) calf serum. CEF were transfected by using a DEAE-dextran procedure described previously (22). Purified plasmid DNA (15 μg) in 6 ml of serum-free SGM made to a final concentration of 0.05 M Tris (pH 7.4) was used to transfect subconfluent 100-mm plates of CEF in the presence of 200 μg of DEAE-dextran per ml. After 30 min at room temperature, 2 ml of the transfection mix was removed, and 10 ml of serum-free SGM was added. The plates were then incubated for 3 h at 37°C, washed with 3 ml of SGM, fed with 10 ml of SGM, and incubated at 37°C. The medium was changed 15 to 20 h later with 10 ml of SGM. NIH 3T3 cells were transfected by calcium phosphate precipitation (13). Plasmid DNA (25 μg) was used for each 150-mm plate. The DNA precipitate was left on the cells for 4 h, and the cells were treated with 1× HEPES-buffered saline containing 20% (vol/vol) glycerol for 4 min as described previously (33).

RNA isolation and analysis. Whole-cell RNA at 48 h after transfection was isolated by the guanidine hydrochloride method essentially as described by Strohman et al. (29). Northern RNA blot analysis with SP6 riboprobes (17) was carried out on formaldehyde-agarose gels (16). The RNase protection mapping was carried out essentially as described previously (28), except that the hybridizations were carried out at 57°C for 14 h and the RNase digestions were done at room temperature for 30 min with 6 μg of RNase A per ml and 300 U of RNase T_1 per ml. The protected fragments were denatured by heating at 85°C for 10 min and separated on a 7 M urea denaturing 6% polyacrylamide gel at 500 V for 3 to 5 h.

Materials. [α-^{32}P]UTP (800 Ci/mmol) was purchased from Amersham Corp., Arlington Heights, Ill. Restriction enzymes, RNase A, RNase T_1, T4 polymerase, T4 ligase, and proteinase K were purchased from Boehringer Mannheim Biochemicals, Indianapolis, Ind. SP6 polymerase was obtained from Promega Biotec Co., Madison, Wis. Plasmid pSP18 was obtained from Bethesda Research Laboratories, Inc., Bethesda, Md.

RESULTS

Characterization of viral mRNAs in transfected NIH 3T3 cells. We first compared the viral RNA produced in CEF and NIH 3T3 cells after transfection of the wild-type Prague A RSV clone, pJD100. Two different tandem radiolabeled riboprobes complementary to sequences spanning each of the major splice sites were used (Fig. 1). After hybridization with these tandem probes and RNase digestion of the resulting hybrids, each complementary probe region (5' region, *env*, and *src*) produced protected fragments of unique size from unspliced RNA and different unique-sized fragments for spliced mRNAs, which were separated by electrophoresis on a polyacrylamide gel. RNase protection results for whole-cell RNA harvested from CEF and NIH 3T3 cells at 48 h after transfection are given in Fig. 2. The origin of the various fragments produced by RNase protection mapping and their sizes in nucleotides are also diagrammed (Fig. 2). In the first set of experiments, the ^{32}P-labeled probe was synthesized from the pMap#10 template (Fig. 2, lanes 5 to 8). No qualitative differences were seen in the mobilities of the protected fragments derived from the 5' region (375 nt unspliced, 143 nt spliced) and the *src* 3'ss region (347 nt unspliced, 276 nt spliced). However, the 180-nt fragment protected by the normal spliced *env* mRNA in CEF cells was absent in the NIH 3T3 lane (Fig. 2, compare lanes 6 and 8). Instead, two other protected *env*

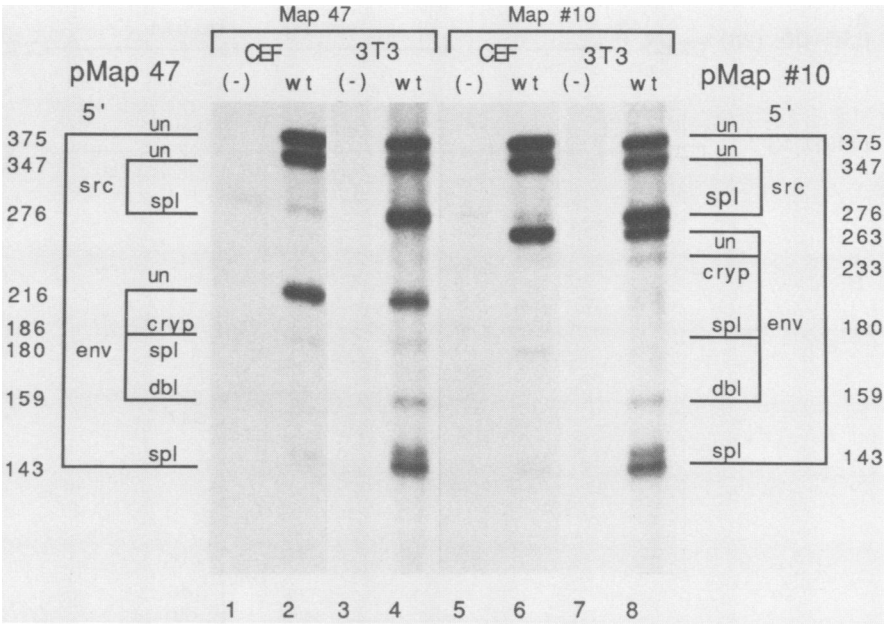

FIG. 2. Comparison of RNase protection maps with RNA from NIH 3T3 cells and CEF transfected with RSV proviral DNA. RNase protection maps with templates pMap47 (lanes 1 through 4) and pMap#10 (lanes 5 through 8). CEF (lanes 1, 2, 5, and 6) were either transfected with pJD100 (lanes 2 and 6) or no DNA (lanes 1 and 5) at 48 h before harvest. Mouse NIH 3T3 cells (lanes 3, 4, 7, and 8) were either transfected with pJD100 (lanes 4 and 8) 48 h before harvest or with no DNA (lanes 3 and 7). The locations and sizes of the fragments protected by riboprobe from pMap47 are indicated on the left; the locations and sizes of fragments protected by riboprobe from pMap#10 are indicated on the right. Note that the bands arising from single-spliced *env* mRNA (*env* spl) and single-spliced RNA arising from splicing at the cryptic splice site (*env* cryp) were not resolved with pMap47 probe. In this and subsequent experiments, 10 μg of CEF RNA and 30 μg of NIH 3T3 RNA were analyzed.

fragments were present whose sizes were approximately 230 and 160 nt. To more clearly resolve the 276-nt spliced *src* and 263-nt unspliced *env* fragments, another probe synthesized from pMap47 (Fig. 1) was used. Note that pMap47 was derived from pMap#10 by deleting 47 nt upstream of the *env* 3′ss, i.e., within the *env* intron. As discussed above with the pMap#10 probe, no qualitative differences in the mobilities of the *src* or 5′ bands were seen with the 3T3 and CEF fragments were compared (Fig. 2, compare lanes 2 and 4). However, the 230-nt *env* band was no longer present. Instead, a band migrating slightly slower than the 180-nt normal *env* spliced band was present (Fig. 2, lane 4). The 160-nt *env* band, however, did not change. The results in Fig. 2 implied that normally spliced *env* mRNA was not detectable in transfected NIH 3T3 cells. The presence of protected fragments not present in CEF suggested that the processing of *env* mRNA might be different in NIH 3T3 cells.

It has been shown in several laboratories that a cryptic 5′ G/GUAAGA (at nt 5237) just downstream from the normal *env* 3′ss (at nt 5078) is activated in avian cells under some circumstances (12, 18, 23). If this cryptic splice site were used to further splice the *env* mRNA in NIH 3T3 cells to form a double-spliced RNA, it would be expected to protect a 159-nt fragment (the distance between the *env* 3′ss at base 5078 and the *env* cryptic 5′ss at nt 5237) with both pMap47 and pMap#10 probes. This size agrees well with the ~160-nt *env*-specific bands seen in the experiments in Fig. 2 (lanes 4 and 8). A single-spliced RNA in which the cryptic 5′ss is used to splice to a downstream 3′ss would be expected (Fig. 1) to protect a 186-nt fragment with the Map47 probe and a 233-nt fragment with the Map#10 probe. The evidence shown in Fig. 2 is consistent with this hypothesis. Note that the 186-nt fragment was not resolved from the 180-nt spliced *env* fragment (Fig. 2, lane 4). However, the absence of the 180-nt band and the appearance of the 233-nt band in the Map#10 probe products (Fig. 2, lane 8) suggests that these bands arise as products of the single-spliced RNA.

We suspected that the most likely splice site to be used as an acceptor for the cryptic 5′ss in *env* would be the *src* 3′ss. As a test to determine whether the *src* 3′ss was used in the cryptic splicing, we constructed a mutant of pJD100, pMPM13, in which the *src* 3′ss was destroyed by a 4-base-pair deletion. The results of RNase mapping with the Map47 probe are given in Fig. 3. Because of a discontinuity due to a second deletion arising downstream of the *src* 3′ss, cleavage of the probe occurred at this site when the hybrid RNAs were digested with nuclease. Cleavage of the probe also occurred at the discontinuity created by the mutation created at the *src* 3′ss (see Materials and Methods). This resulted in the production of three protected *src* probe fragments arising from unspliced RNA. The positions of two of these fragments (148 and 130 nt) are indicated in Fig. 3, a third, smaller fragment (71 nt) is not shown. In addition, a minor band at the position of the normal spliced *src* probe (276 nt) resulted from incomplete RNase digestion. In addition to these bands arising from unspliced *src*, the normal expected 5′-specific protected bands (375 and 143 nt), and the unspliced *env* band (216 nt), a band migrating at the normal spliced *env* position at 180 nt was present. The mobility of this fragment was not altered when the RNA was analyzed by using a riboprobe generated from pMap#10 rather than pMap47 (data not shown). Thus, when the *src* 3′ss was deleted, normal single-spliced *env* mRNA was formed. The band at approximately 160 nt (arrow in Fig. 3), which was diagnostic for splicing from the cryptic 5′ss, was

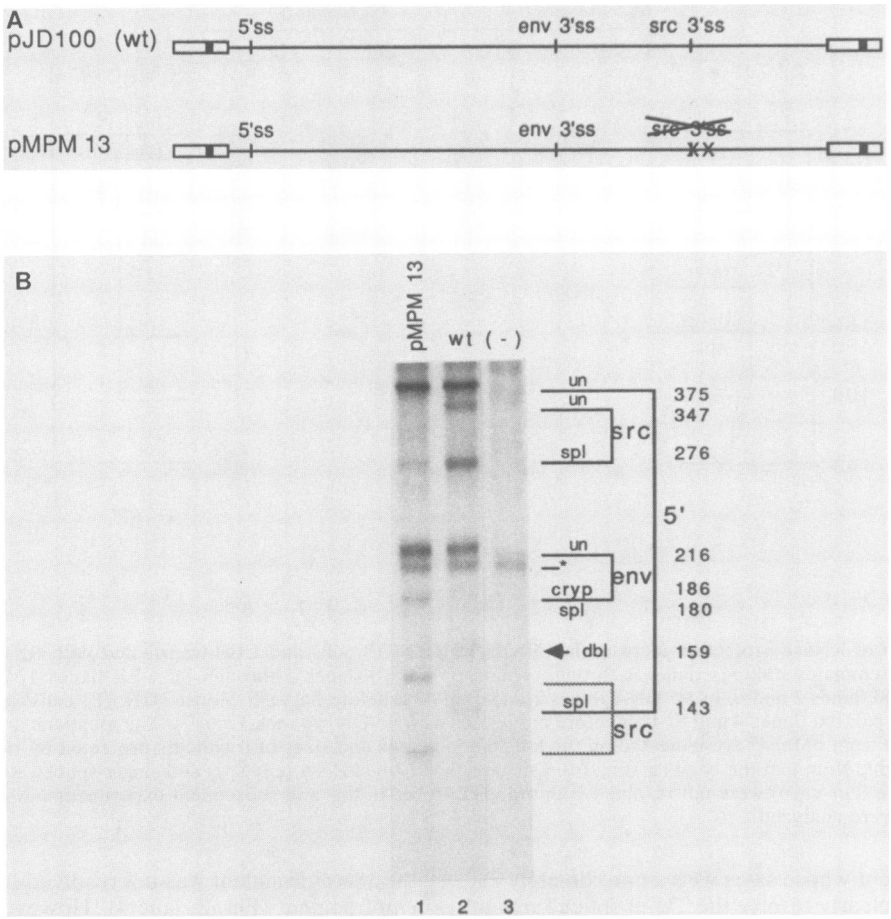

FIG. 3. Effects of inactivation of the *src* 3′ss on *env* splice site usage in NIH 3T3 cells. (A) Schematic representation of the plasmids used in this experiment. (B) RNase protection map with a probe from pMap47 and RNAs isolated from NIH 3T3 cells transfected with pMPM13 (lane 1), pJD100 (lane 2), and no DNA (lane 3). The identities and locations of the various protected fragments are indicated. Labeling of bands is as described in the legend to Fig. 2. The asterisk (*) indicates a background band found in the control RNA. The two smaller *src*-specific bands arising from unspliced (un)RNA in pMPM13 transfected cells are also indicated and migrate faster and slower than the 143-nt spliced 5′ band. The position of the 160-nt fragment diagnostic for the double-spliced RNA is indicated by an arrow.

not detectable. These results indicate that formation of the double-spliced mRNA from the *env* cryptic 5′ss requires the *src* 3′ss.

Evidence for the presence of double-spliced RNA species in NIH 3T3 cells was also obtained by Northern blot analysis. A ^{32}P-labeled riboprobe specific for the *env* splice site region was prepared and used to probe the Northern blots (Fig. 4). A band at ~4.0 kilobases (kb) was present in all lanes, including the negative control lanes; this band corresponded to the position of 28S rRNA as determined by ethidium bromide staining. Attempts to remove the nonspecific binding of this probe by RNase digestion and further washing of the blot resulted in the loss of the virus-specific signals as well. We do not understand the reason for the affinity to 28S rRNA. However, since the position of the 28S rRNA did not overlap the positions of the specific viral mRNAs, the artifact band did not interfere with the analysis of the viral RNAs. RNA from wild-type pJD100-transfected cells hybridized to the *env*-specific probe is shown in Fig. 4, lane 1. Two specific bands were detected, a 9.3-kb band corresponding to the full-length unspliced RNA and a 2.8-kb band corresponding to the double-spliced mRNA, which is slightly larger than normal *src* mRNA. A specific band was

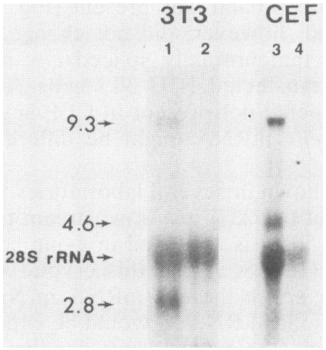

FIG. 4. Northern blot analysis of mouse NIH 3T3 cells transfected with cloned DNA. Whole-cell RNA was isolated 48 h after transfection and fractionated on an 1.2% agarose–formaldehyde gel. RNA isolated from NIH 3T3 cells (lane 1) and CEF (lane 3) transfected with pJD100 or the same cells with no DNA (lanes 2 and 4) were electrophoresed and probed with a ^{32}P-labeled riboprobe specific to the *env* splice site (the same region protected by the *env* portion of pMap47). The amounts of RNA applied to the gel were 30 μg in lanes 1 and 2 and 10 μg in lanes 3 and 4.

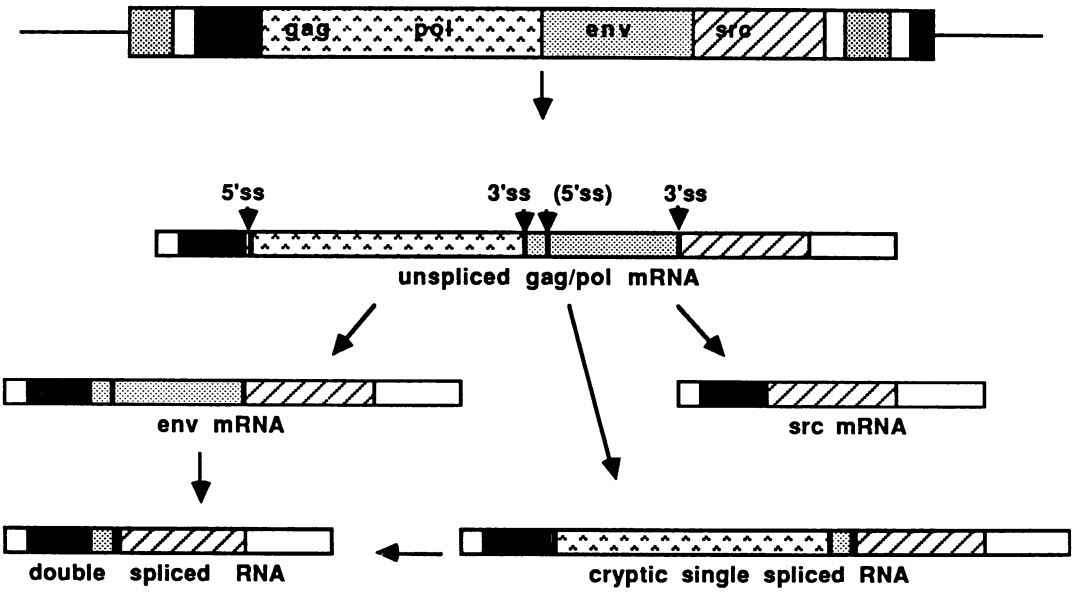

FIG. 5. Diagram showing the origin of viral mRNAs present in mouse NIH 3T3 cells transfected with pJD100. Note that each of the RNA species contains a common 5' leader composed of sequence from R (□) and U5 (■) of the long terminal repeat as well as the noncoding sequence between U5 and the *gag* AUG (■). The major 5'ss, *env*, and the *src* 3'ss are shown. The cryptic 5'ss is shown within parentheses.

not visible at the position of normal *env* mRNA (4.6 kb) which migrated slower than the ~4.0-kb rRNA background band (Fig. 4). The results of a Northern blot of RNAs from pJD100 (lane 3) and mock-transfected CEF (lane 4) are also given in Fig. 4. Specific bands of 9.3 and 4.6 kb were present, corresponding to the full-length unspliced and normal single-spliced *env* RNAs, respectively. Confirming the results of the RNase protection assays (Fig. 2), a specific double-spliced *env*-containing RNA band at the position of the *src* mRNA (2.6 kb) was not detected in transfected CEF.

Thus, our results suggest that RSV RNA is processed in NIH 3T3 cells (Fig. 5). A minor (cryptic) 5'ss is located in the 5' region of the *env* gene, probably at the consensus sequence beginning at nt 5237 since this is the only potential consensus splice donor site in this region of the RSV genome. Use of this cryptic 5'ss and the *src* 3'ss in NIH 3T3 cells resulted in the formation of both a double-spliced mRNA and a single-spliced mRNA.

Comparison of amounts of spliced and unspliced viral RNAs in transfected CEF and NIH 3T3 cells. It was obvious from the results given in Fig. 2 that there were significant quantitative differences between NIH 3T3 cells and CEF in the relative amounts of the spliced products. The overall level of splicing, as determined by fragments derived from the 5' region of the tandem riboprobe (for both pMap47 and Map#10, the 375- and 143-nt fragments), is clearly increased in NIH 3T3 cells. Most of the increased splicing occurred at the *src* 3'ss, as can be seen by comparing the relative amounts of the 276-nt spliced *src* fragments in CEF and NIH 3T3 cells (Fig. 2, compare lanes 2 and 4 and lanes 6 and 8). The autoradiograms from a number of separate experiments were scanned, and the relative molar amounts of spliced and unspliced RNA transcripts were determined (Table 1). In the case of CEF, the overall extent of viral RNA splicing was determined to be approximately 25%. In NIH 3T3 cells, on the other hand, the extent of splicing was considerably higher, approximately 60 to 70%. The double-spliced RNA comprised about 7%, and the RNA that was singly spliced from the cryptic 5'ss to the *src* 3'ss comprised about 3%, of the total viral RNA in NIH 3T3 cells transfected with pJD100. From these values, the amount of normal single-spliced *src* mRNA was calculated to be approximately 50 to 60% of the total viral RNA, i.e., the difference between the number of RNA molecules spliced at the *src* 3'ss and the number of RNA molecules resulting from the cryptic splicing in *env*. It is of interest that the fraction of total viral RNA spliced at the *env* 3'ss was not significantly different in NIH 3T3 cells and CEF (11 versus 13%). However, the fraction of single- and double-spliced RNA spliced at the *src* 3'ss was increased approximately fivefold in NIH 3T3 cells (63 versus 13%).

It appeared from the Northern blot data (Fig. 4, lane 1) that the *env* probe hybridized more strongly to the 2.8-kb RNA than to the full-length 9.3-kb RNA. This is clearly inconsistent with the RNase protection data given in Table 1. We believe that this discrepancy arises because of less

TABLE 1. Relative amounts of viral RNA species in CEF and NIH 3T3 cells transfected with RSV proviral DNA[a]

RNA	% CEF ± SD	% NIH 3T3 cells ± SD
Unspliced	74.1 ± 4.0	37.3 ± 4.7
Single-spliced *src*	13.0 ± 2.6	51.6 ± 4.3
Single-spliced *env*	12.8 ± 2.3	ND[b]
Double-spliced *env*	ND	7.6 ± 2.0
Cryptic single-spliced *env*	ND	3.6 ± 1.2

[a] For CEF RNA, the integrated values obtained by densitometric measurements for the unspliced *env*, spliced *env*, and spliced *src* bands were determined (Fig. 1). For NIH 3T3 RNA, the integrated values for the cryptic single and double-spliced bands were also determined. The integrated values were normalized for the appropriate base compositions of the bands, and the molar ratios of each RNA species were determined. The percentage of the total viral RNA for each RNA was then calculated. For the NIH 3T3 cells, the contribution of the cryptic spliced *env* species (double and single spliced) was subtracted from the *src* band value. Standard deviations are based on 10 determinations for CEF and 7 determinations for NIH 3T3 cell RNA.

[b] ND, Not detected.

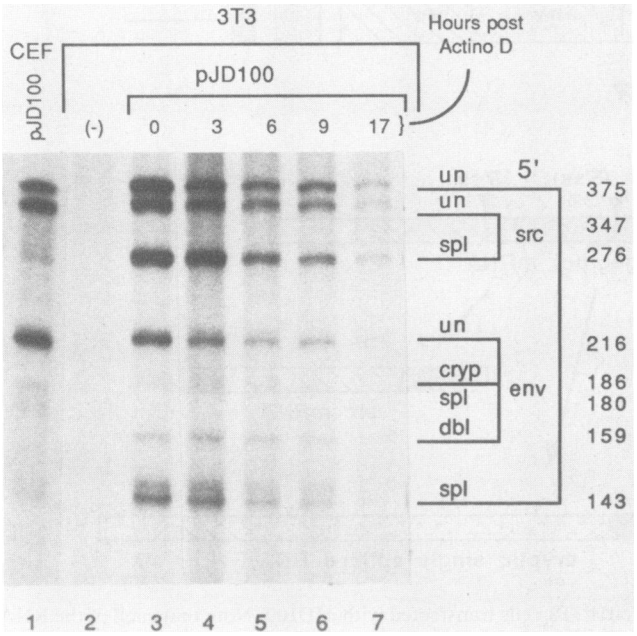

FIG. 6. Stabilities of the various viral RNAs identified in mouse NIH 3T3 cells transfected with pJD100. RNase protection mapping experiment with a riboprobe from pMap47 and RNAs from NIH 3T3 cells transfected with pJD100 and harvested at the following times after the addition of dactinomycin (Actino D) (1 μg/ml) (lanes): 3, 0 h; 4, 1 h; 5, 3 h; 6, 6 h; 7, 9 h; 8, 17 h. RNA from CEF transfected with pJD100 is shown in lane 1 as a positive control, and RNA from mock-transfected NIH 3T3 cells is shown in lane 2 as a negative control. The locations and identities of the protected bands are indicated and are as described in the legend to Fig. 2.

efficient transfer of higher-molecular-weight RNA species in the Northern blot procedure. In fact, we have noted considerable differences in the relative intensities of the two bands in different Northern blot experiments (data not shown). Thus, our data indicate that the RNase protection assay is the more appropriate method to obtain accurate quantitative data of viral RNA levels.

It was difficult to directly compare the total levels of RNA transcripts in CEF and NIH 3T3 cells since the amount of DNA transfected, the transfection protocol, and the exposure times of the autoradiograms were different. However, based on the data of Fig. 1 as well as other experiments, we estimated that the level of viral RNA in transfected cells was 10- to 20-fold lower in NIH 3T3 cells than in CEF. This is in agreement with other studies showing reduced levels of viral RNA in RSV-transformed mammalian cell lines (3, 6, 19).

Comparison of stabilities of RSV RNA in NIH 3T3 cells and CEF. It was possible that the relatively larger amount of spliced RNA compared with the amount of unspliced RNA in NIH 3T3 cells (Table 1) might be due to the instability of the unspliced RNA in NIH 3T3 cells versus CEF rather than to the differences in RNA splicing. Indeed, the lability of unspliced RNA transcribed from certain RSV *gag* mutants is responsible for reduced ratios of unspliced to spliced RNA in CEF (2). To measure RNA stabilities, NIH 3T3 cells were transfected for 48 h with wild-type pJD100 and then treated with dactinomycin (1 μg/ml) to inhibit further transcription. Whole-cell RNA was then harvested at various times (Fig. 6). It was indicated in previously reported results from this laboratory that in CEF the *env* mRNA is most stable (half-life, ~15 h), the *src* mRNA is moderately stable (half-life, ~10 h), and the genomic unspliced message is the most labile (half life, ~8 h) (27). In the experiment shown in Fig. 6 the *src* mRNA appeared to be the least stable (half-life, ~4 h) in NIH 3T3 cells; the unspliced message was slightly more stable (half-life, ~4.5 h). As shown above, we were unable to detect any normal *env* mRNA in NIH 3T3 cells. The two mRNAs resulting from the use of the cryptic splice site appeared to have stabilities greater than that of the other viral RNAs. Overall, the RSV RNA was less stable in NIH 3T3 cells than in CEF. From these data we conclude that the observed steady-state ratios of spliced to unspliced RNA in NIH 3T3 cells are likely to underestimate the actual extent of the splicing because the unspliced RNA is more stable than the major spliced species, the *src* mRNA.

DISCUSSION

We have obtained evidence for altered splicing of RSV RNA in mouse NIH 3T3 fibroblasts compared with RSV RNA in CEF. We have demonstrated a significant quantitative shift in the distribution of viral mRNAs toward shorter spliced mRNAs 48 h after transfection. RSV RNA has been shown to be mostly spliced in RSV-transformed mammalian cell lines (8, 9, 19). Experiments from this laboratory have indicated that the types of mRNA and the extent of RNA splicing are identical in CEF transiently transfected by cloned viral DNA and in CEF synchronously infected by virus at a high multiplicity of infection (Berberich and Stoltzfus, unpublished data). Therefore, RNA processing of viral RNA in transfected cells appears to accurately reflect events in virus-infected cells. Our results suggest that the preponderance of spliced mRNA in mammalian cells does not reflect genetic selection for an overspliced phenotype in rare transformed cells, since this also occurs in transient expression assays without selection for transformation. The extent of splicing may be even higher than that indicated by the steady-state ratios of spliced to unspliced RNA, since the *src* mRNA, which is the major spliced species in NIH 3T3 cells (Table 1), appears to be less stable than the unspliced RNA in NIH 3T3 cells.

Our results further indicate that qualitative differences exist in permissive CEF versus nonpermissive mammalian cells. We have shown that normal *env* mRNA is not detectable in the RSV DNA-transfected NIH 3T3 cells. Instead, we have obtained evidence for two novel spliced RNA species, a 2.8-kb double-spliced mRNA derived by further splicing of *env* mRNA and smaller amounts of a 7.5-kb single-spliced RNA (Fig. 5). Processing of both of these RNAs utilizes a cryptic 5′ss, which appears to be at the splice consensus sequence beginning at nt 5237 within the *env* coding sequence. This 5′ss has been used previously (12, 18, 23). The transformation-defective RSV deletion mutant *td*109 is believed to acquire c-*src* by splicing from the cryptic 5′ss in *env* to the first exon of c-*src* in infected chickens (23). Fung et al. (12) found that the *env* cryptic 5′ss was involved in the induction of erythroblastosis by proviral insertion of avian leukosis virus within the cellular c-*erbB* locus. RNA transcripts initiated at the avian leukosis virus 5′ long terminal repeat were spliced from the cryptic 5′ss in *env* to a 3′ss within c-*erbB*. Finally, a recombinant RSV-based retroviral vector carrying the c-*erbB* cDNA produced two c-*erbB* mRNAs. One of these mRNAs is directly spliced from the major 5′ss in *gag* to the c-*erbB* 3′ss; the other is double spliced from the *gag* 5′ss to the *env* 3′ss and further spliced from the *env* cryptic 5′ss to the c-*erbB* 3′ss (18). Thus, although we did not detect spliced RNAs by using the

cryptic 5'ss in CEF, it is clear that under some circumstances and in some tissues the cryptic splice site can be used in chicken cells, and our results cannot exclude the presence of minor amounts of such RNA. The cryptic splice site in *env* could be used to create novel mRNAs in which the *env* signal peptide sequence is fused to downstream open reading frames by using cryptic 3'ss within the *env* and *src* genes. Further studies with more sensitive techniques are required to obtain evidence for such putative mRNAs.

It is possible that the presence of double-spliced mRNA in NIH 3T3 cells may affect *src* gene expression. The 5' leader of the normal *src* mRNA contains four short upstream open reading frames; the 5' distal upstream open reading frame is initiated by the *gag/env* AUG (4, 30). However, the double-spliced mRNA appears to be identical to normal *src* mRNA, except for an in-frame insertion of the leader portion of the *env* mRNA, which includes the signal peptide sequence. If *src* can, indeed, be translated from the double-spliced mRNA by reinitiation, translation of the upstream orf may have effects on downstream *src* expression. For instance, RSV *env* mRNA is known to be associated with membrane-bound polysomes, whereas *src* mRNA is associated with cytoplasmic polysomes (14). If the double-spliced mRNA were distributed like the *env* mRNA, it could conceivably affect the cellular targeting of $pp60^{src}$ synthesized by the two types of mRNA. Further work however must be done to fully characterize the double-spliced mRNA.

The absence of normal *env* mRNA shown above in transfected NIH 3T3 cells may explain in part the nonpermissiveness of mouse cells to infection by RSV. However, this is clearly not the only defect preventing virus replication. Wills et al. (38) have recently shown that the RSV *gag* precursor is not transported to the cytoplasmic membrane of mammalian cells and that this defect can be corrected by altering the N terminus to allow N-terminal myristylation. This mutation, however, when inserted back into an infectious RSV plasmid and transfected into mammalian cells, did not result in productive virus infection (J. Wills, personal communication). The level of transcription from the RSV long terminal repeat, as we have confirmed in this study in transiently transfected NIH 3T3 cells, has also been shown to be considerably lower in mammalian cells compared with the level in CEF (3, 6, 19). Therefore, defective mRNA splicing, lower proviral transcription, and inefficient protein processing may act synergistically to completely block virus replication in mammalian cells.

ACKNOWLEDGMENTS

This work was supported by Public Health Service grant CA28051 from the National Cancer Institute and by the Veterans Administration. S.L.B. was supported by Public Health Service National Research Service Award GM07091 from the National Institute of General Medical Sciences. L.P.T. was supported by a Career Award from the Veterans Administration.

We thank M. Stinski for critical reading of the manuscript and M. Reeve for typing.

LITERATURE CITED

1. **Altaner, C., and H. M. Temin.** 1970. Carcinogenesis by RNA sacroma viruses. XII. A quantitative study of infection of rats *in vitro* by avian sarcoma viruses. Virology **40**:118–134.
2. **Arrigo, S., and K. Beemon.** 1988. Regulation of Rous sarcoma virus RNA splicing and stability. Mol. Cell. Biol. **8**:4858–4867.
3. **Bishop, J. M., C.-T. Deng, B. W. J. Mahy, N. Quintrell, E. Stavnezer, and H. E. Varmus.** 1976. Synthesis of viral RNA in cells infected by avian sarcoma viruses, p. 1–20. *In* D. Baltimore, A. S. Huang, and C. F. Fox (ed.), Animal virology, vol. 4. Academic Press, Inc., New York.
4. **Chang, L.-J., and C. M. Stoltzfus.** 1985. Cloning and nucleotide sequences of cDNAs spanning the splice junctions of Rous sarcoma virus mRNAs. J. Virol. **53**:969–972.
5. **Coffin, J. M.** 1972. Rescue of Rous sarcoma virus from Rous sarcoma virus-transformed mammalian cells. J. Virol. **10**: 153–156.
6. **Coffin, J. M., and H. M. Temin.** 1972. Hybridization of Rous sarcoma virus DNA polymerase product and RNA from chicken and rat cells infected with Rous sarcoma virus. J. Virol. **9**:766–775.
7. **Cooper, G. M., N. G. Copeland, A. D. Zelenetz, and T. Krontiris.** 1979. Transformation of NIH-3T3 mouse cells by avian retrovirual DNAs. Cold Spring Harbor Symp. Quant. Biol. **44**:1169–1176.
8. **Deng, C.-T., D. Boettiger, I. Macpherson, and H. E. Varmus.** 1974. The persistance and expression of virus-specific DNA in revertants of Rous sarcoma virus-transformed BHK-21 cells. Virology **62**:512–521.
9. **Deng, C.-T., D. Stehelin, J. M. Bishop, and H. E. Varmus.** 1977. Characteristics of virus-specific RNA in avian sarcoma virus-transformed BHK-21 cells and revertants. Virology **76**:313–330.
10. **Duff, R. G., and P. K. Vogt.** 1969. Characteristics of two new avian tumor virus subgroups. Virology **39**:18–30.
11. **Eisenman, R. N., and V. M. Vogt.** 1978. The biosynthesis of oncovirus proteins. Biochim. Biophys. Acta **473**:187–239.
12. **Fung, T., W. G. Lewis, H.-J. Kung, and L. B. Crittenden.** 1983. Activation of the cellular oncogene c-erbB by LTR insertion: molecular basis for induction of erythroblastosis by avian leukosis virus. Cell **33**:357–368.
13. **Graham, F. L., and A. J. van der Eb.** 1973. A new technique for the assay of infectivity of human adenovirus 5 DNA. Virology **52**:456–467.
14. **Lee, J. S., H. E. Varmus, and J. M. Bishop.** 1979. Virus-specific messenger RNAs in permissive cells infected by avian sarcoma virus. J. Biol. Chem. **245**:8015–8022.
15. **Machala, O., L. Donner, and J. Svoboda.** 1970. A full expression of the genome of Rous sarcoma virus in heterokaryons formed after fusion of virogenic mammalian cells and chicken fibroblasts. J. Gen. Virol. **8**:219–229.
16. **Maniatis, T., E. F. Fritsch, and J. Sambrook.** 1982. Molecular cloning: a laboratory manual. Cold Spring Harbor Laboratory, Cold Spring Harbor, N.Y.
17. **Melton, D. A., P. A. Krieg, M. R. Rebagliati, T. Maniatis, K. Zinn, and M. R. Green.** 1984. Efficient in vitro synthesis of biologically active RNA and RNA hybridization probes from plasmids containing a bacteriophage SP6 promoter. Nucleic Acids Res. **12**:7035–7056.
18. **Pelley, R. J., C. Moscovici, S. Hughes, and H.-J. Kung.** 1988. Proviral-activated c-*erb*B is leukemogenic but not sarcomagenic: characterization of a replication-competent retrovirus containing the activated c-*erb*B. J. Virol. **62**:1840–1844.
19. **Quintrell, N., S. H. Hughes, H. E. Varmus, and J. M. Bishop.** 1980. Structure of viral DNA and RNA in mammalian cells infected with avian sarcoma virus. J. Mol. Biol. **143**:363–393.
20. **Schwartz, D. E., R. Tizard, and W. Gilbert.** 1983. Nucleotide sequence of Rous sarcoma virus. Cell **32**:853–869.
21. **Simcovic, D.** 1972. Characteristics of tumors induced in mammals, especially rodents, by viruses of the avian sarcoma, leukosis group. Adv. Virus Res. **17**:95–127.
22. **Sompayrac, L. M., and K. J. Danna.** 1981. Efficient infection of monkey cells with DNA of SV40. Proc. Natl. Acad. Sci. USA **78**:7575–7578.
23. **Soong, M.-M., S. Iijima, and L.-H. Wang.** 1986. Transduction of c-*src* coding and intron sequences by a transformation-defective deletion of Rous sarcoma virus. J. Virol. **59**:556–563.
24. **Steimer, K. S., and D. Boettiger.** 1977. Complementation rescue of Rous sarcoma virus from transformed mammalian cells by polyethylene glycol-mediated cell fusion. J. Virol. **23**:133–141.
25. **Stoltzfus, C. M.** 1988. Synthesis and processing of avian sarcoma retrovirus RNA. Adv. Virus Res. **35**:1–38.
26. **Stoltzfus, C. M., L.-J. Chang, T. P. Cripe, and L. P. Turek.** 1987. Efficient transformation by Prague A Rous sarcoma virus

plasmid DNA requires the presence of *cis*-acting regions within the *gag* gene. J. Virol. **61**:3401–3409.
27. **Stoltzfus, C. M., K. Dimock, S. Horikami, and T. A. Ficht.** 1983. Stabilities of avian sarcoma virus RNAs: comparison of subgenomic and genomic species with cellular mRNAs. J. Gen. Virol. **64**:2191–2202.
28. **Stoltzfus, C. M., and S. J. Fogarty.** 1989. Multiple regions in the Rous sarcoma virus *src* gene intron act in *cis* to affect the accumulation of unspliced RNA. J. Virol. **63**:1669–1676.
29. **Strohman, R., P. Moss, J. Micou-Eastwood, D. Spector, A. Przybyla, and B. Peterson.** 1977. Messenger RNA for myosin polypeptides: isolation from single myogenic cell cultures. Cell **10**:265–273.
30. **Swanstrom, R., R. C. Parker, W. E. Varmus, and J. M. Bishop.** 1983. Transduction of a cellular oncogene: the genesis of Rous sarcoma virus. Proc. Natl. Acad. Sci. USA **80**:2519–2523.
31. **Svoboda, J., and R. Dormashkin.** 1969. Rescue of Rous sarcoma virus from virogenic mammalian cells associated with chicken cells and treated with Sendai virus. J. Gen. Virol. **4**:523–529.
32. **Svoboda, J., O. Machala, L. Donner, and V. Sovova.** 1971. Comparative study of RSV rescue from RSV-transformed mammalian cells. Int. J. Cancer **8**:391–400.
33. **Turek, L. P., and H. Oppermann.** 1980. Spontaneous conversion of nontransformed avian sarcoma virus-infected rat cells to the transformed phenotype. J. Virol. **35**:466–478.
34. **Varmus, H. E., J. M. Bishop, and P. K. Vogt.** 1973. Appearance of virus-specific DNA in mammalian cells following transformation by Rous sarcoma virus. J. Mol. Biol. **74**:613–626.
35. **Varmus, H. E., P. K. Vogt, and J. M. Bishop.** 1973. Integration of DNA specific for Rous sarcoma virus after infection of permissive and nonpermissive hosts. Proc. Natl. Acad. Sci. USA **70**:3067–3071.
36. **Vogt, V. M., D. A. Bruckenstein, and A. P. Bell.** 1982. Avian sarcoma virus *gag* precursor polypeptide is not processed in mammalian cells. J. Virol. **44**:725–730.
37. **Von der Helm, K., J. Kempeni, W. Willie, and K. Willecke.** 1980. Rous sarcoma virus precursor protein Pr76 is processed in avian sarcoma virus-transformed mammalian cells after fusion-injection of viral protein p15. Virology **106**:310–316.
38. **Wills, J. W., R. C. Craven, and J. A. Achacoso.** 1989. Creation and expression of myristylated forms of Rous sarcoma virus *gag* protein in mammalian cells. J. Virol. **63**:4331–4343.